CHARACTERISING AND MODELLING TOOL-PLY FRICTION OF VISCOUS TEXTILE COMPOSITES

Philip Harrison[1], Hua Lin[2], Mark Ubbink[3], Remko Akkerman[3],
Karin van de Haar[3], Andrew C. Long[2]
[Philip Harrison]: p.harrison@mech.gla.ac.uk
[1]Department of Mechanical Engineering, University of Glasgow, G12 8QQ
[2]University of Nottingham
[3]University of Twente

Keywords: Friction, Viscous Textile Composite

Abstract

The first part of the paper describes two experimental methods for measuring the tool-ply friction behaviour of impregnated thermoplastic textile composites. These include the so-called pull through test and tests conducted using a commercial rheometer using a custom designed platen. Results from the two techniques are compared and the relative advantages and disadvantages of the different test methods are discussed. Data produced over a range of temperatures, normal pressures and shear rates using the rheometer are employed to produce a master equation for the steady state friction. The method of shifting the data to produce this empirically determined equation is described.

In the second part of the paper, a predictive meso-scale model is presented that incorporates parameters such as fabric architecture, tow geometry and matrix viscosity. The model is based on lubrication theory and can predict steady state friction. Predictions from the model are compared with experimental results.

1 Introduction

Press forming of thermoplastic textile composites is potentially a fast and efficient method of production. However, while stretch forming and deep-drawing of sheet metal is today a relatively well understood process supported by sophisticated CAE tools, the same cannot yet be said for textile composites. As such a large research effort is underway to create equivalent CAE tools for these materials.

The manufacture of textile composite components of potentially complex double curvature geometries involves a forming stage in which dry or impregnated reinforcement takes the required shape through 'press forming' or 'deep drawing' processes. Wrinkling of the sheet during forming is an unwanted defect and can be inhibited via in-plane tension induced in the sheet using a 'blank-holder' [1, 2]. Friction occurring between the composite material and metal tooling during forming imparts tensile stresses in the material. These tensile stresses can help to counteract compressive stresses that may be generated during forming due to deformation of the material. Such compressive stresses could otherwise cause ply buckling and wrinkling.

Prior investigation has shown that for pre-impregnated textile composites, process parameters including normal pressure, velocity and matrix viscosity (related to temperature) all affect the friction between material and tooling. Since this plays a direct role in determining the amount of in-plane tension induced in the sheet during forming it is vital to characterise and model this friction behaviour if accurate finite element simulations of the process are to be conducted.

2 Material

A 2 x 2 twill weave pre-consolidated thermoplastic, textile composite, Vetrotex Twintex®, consisting of commingled E-glass and polypropylene (PP) yarns has been tested. The material had a nominal thickness of 0.5 mm and a fibre volume fraction of 0.35. A photograph of the material is shown in Fig. 1. The unit cell measures approximately 20 x 20 mm. The tow geometry is one of the inputs in the meso-scale model.
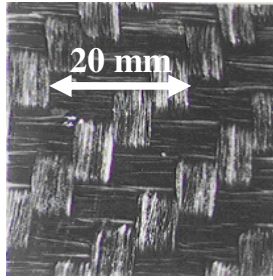
Fig 1. 2 x 2 Twintex® glass-polypropylene preconsolidated sheet.

3 Experimental Methods

Various methods for characterising the friction of fabric sheets, considering effects of normal pressure, temperature and sliding speed have been devised [4-11]. In this investigation two different techniques have been used. Hands-on experience with each of these methods is useful when discussing the relative merits of each.

3.1 Pull-through rig

The first experimental method employed is based on a design first used by Wilks [5]. It is referred to here as a 'pull-through' rig to distinguish it from similar 'pull-out' designs [4,6,7,9,10]. A photograph of the rig is shown in Fig 2 together with a schematic of the top view of the rig.
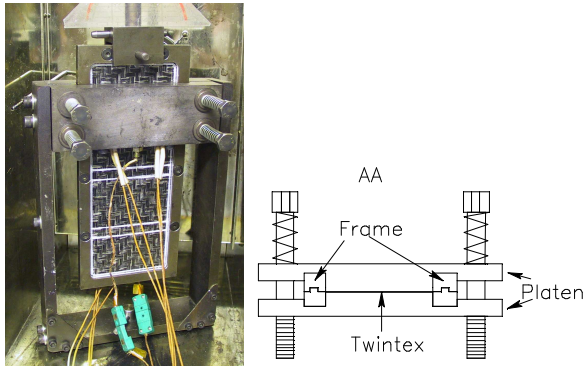
Fig 2. Left: Photo of pull through rig in oven. Right: Schematic of rig viewed from above.

The rig consists of a steel frame approximately 300 x 200 mm with two steel platens, 175 x 25 x 6 mm constituting the top member of the frame. A second frame (specimen frame) secures the specimen and is connected to the load cell at the topmost point. This frame moves through grooves that were milled on the adjacent faces of both steel platens. The test material is secured in the specimen frame and pulled between the two steel platens. The bottom edge of each platen is milled to prevent snagging of the specimen as it enters between the platens. The contact area between platen and material is 89 x 63 mm (area = $5607mm^2$). Two 50 W cartridge heaters per platen heat the platens to the test temperature, which is regulated by a feedback loop with two K-type thermocouples. The normal pressure on the platens is provided by four springs. The specimen is the same size as the outer perimeter of the specimen frame. In order to heat material initially outside of the platens, the entire rig is placed in a Hounsfield Environment Chamber (oven) and heated to the same temperature as the heated platens. Thus, the intention was that the temperature of both the oven and platens should be identical and testing would be as close to isothermal as possible. The specimen frame is connected to the crosshead of a PC-controlled Hounsfield H25k-S Universal testing Machine, fitted with a 2.5 kN load cell. The test specimens can only be tested in a 0° or 90° configuration otherwise the frame is unable to clamp the specimen securely enough during testing. Each experiment was conducted at least three times.

3.2 Rheometer

An alternative method of measuring friction has been employed by adapting a commercial rheometer. Experiments were performed on a Bohlin CVOR200 Rheometer with Extended Temperature Cell (ETC) oven (see Fig. 3). All tests were conducted in a nitrogen atmosphere to minimize polymer degradation. The rheometer was fitted with a custom designed rig that allowed the textile composite sheet to be held firmly in place during testing. The rig consists of a pair of parallel stainless steel platens, the lower platen was a truncated cone with a diameter of 25 mm. The upper platen was a flat disk with diameter 40 mm (Figs. 4 & 5).

Fig 3. Bohlin rheometer with fitted Extended Temperature Cell (ETC)
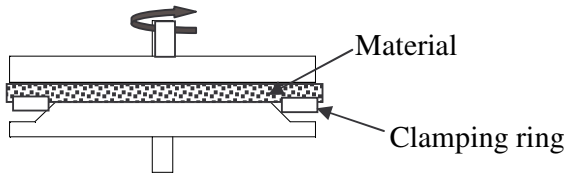
Fig. 4. Side profile of custom made fixture with loaded sample.

Fig. 5. Photograph of custom designed platens.

A specimen is cut appropriately (see Fig. 6) and placed between the upper platen and a clamping ring (outer diameter of 40mm and inner diameter of 30mm). Four small screws are used to clamp the ring and specimen in position. The screws secure the specimen by passing through the ring and into the upper platen. The specimen is then placed in the ETC (oven) and heated. After the specimen reaches the required temperature, the upper platen with the specimen is positioned in the rheometer parallel with the lower platen. A normal force is set on the specimen by lowering the upper platen against the lower platen. The value of the normal force is monitored by the computer.
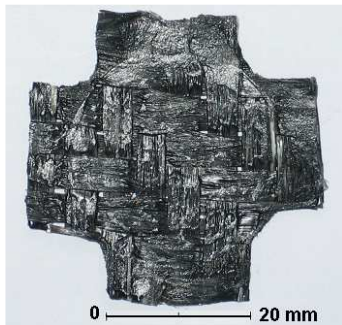
Fig. 6. Example of a test sample following testing. The arms of the specimen are fastened under the clamping ring.

4 Results

Summarised results from the two different test methods are presented below. The effects of rate, normal force and temperature (hence matrix viscosity) are examined. The general trends in the data are summarized and the relative advantages and disadvantages of the two methods are discussed.

4.1 Pull-through rig

Typical results from experiments performed at a normal pressure of 0.036 MPa are shown in Fig. 7. The temperature during each experiment was kept constant at 180°C.
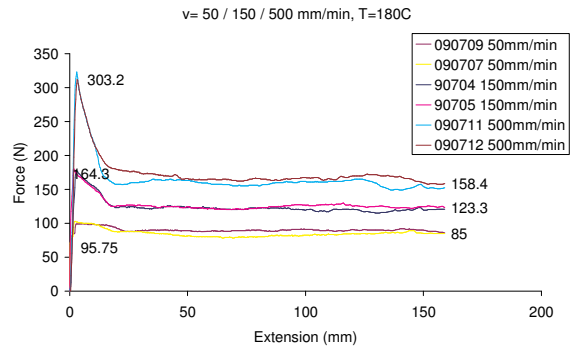
Fig 7. Typical results from the Pull-though rig tests conducted at 3 rates using a pressure of 0.036 MPa.

Table 1. Peak and steady friction values measured under various experimental conditions.

T=180 deg C	Normal force = 67N	
Rate (mm/min)	μ (peak)	μ (steady)
10	-	0.22
50	0.64	0.37
150	0.97	0.40
500	1.56	0.43
T=180 deg C	Normal Force = 135N	
Rate (mm/min)	μ (peak)	μ (steady)
50	0.23	0.21
150	0.41	0.31
500	0.75	0.39
T=180 deg C	Rate = 150 mm/min	
Normal force (N)	μ (peak)	μ (steady)
67	0.98	0.45
135	0.54	0.36
202	0.46	0.3

The force versus displacement curves show peak values followed by steady state values. Thus, both peak and steady state friction behaviours are evident and both follow the same general trends. These included increasing friction coefficients with increasing rate, and decreasing friction coefficients for increasing normal force and temperature. These same trends have been reported previously for other types of Twintex [7, 9]. Table 1 summarises the friction behaviour under various experimental conditions. Note that for T = 180°C and a normal force of 67N no peak friction was observed. Also, at higher rates (150 & 500 mm/min) steady state friction showed large variability and was less reliable. This was thought to be due to the thermal gradient found to exist between the top and bottom of the environmental chamber. Measurements showed that the temperature at the bottom of the environmental chamber could be up to 30°C lower than at the top of the chamber, even when using the convection fan. For slow rates this was not so problematic as the electrically heated platens had sufficient time to heat the specimens to the correct temperature as they moved against the metal. At higher rates the heating time decreased causing large variations in the higher rate data.

The test method was found typically to require between 40-60 minutes for each test making collection of a large amount of data a laborious and costly process. Furthermore, test repeatability was rather poor. To overcome these limitations, a novel experimental technique, involving the use of a commercial rheometer, is proposed and evaluated.

4.2 Rheometer results

Using the rheometer is was possible to generate data at a much faster rate than when using the pull-though test rig. This meant a much larger test matrix could be completed in a reasonable amount of time, presenting the possibility of generating a master curve incorporating rate, normal force and temperature. This involves shifting the data produced under different experimental conditions such that the whole body of data can be described using a single equation. In order to do this, suitable shifting factors must be determined.

The input data in the rheometer are normal force, shear stress and temperature. Experiments were performed over a range of normal forces (2.5, 10, 20, 50 and 90% of the maximum force that could be applied by the rheometer, i.e. 19.6 N), at various imposed shear stresses (500, 1100, 2000 and

5000Pa) and for several temperatures (160, 180, 200 and 220°C). Each test was repeated three times and average results were used for data processing.

It was found that during the experiments the normal force changed due to lateral flow of the sample. Thus normal force was one of the outputs from the test. Other outputs included rotation angle and time. A typical test result is shown in Fig. 8 which shows angular displacement versus time for a given imposed constant torque (constant shear stress).
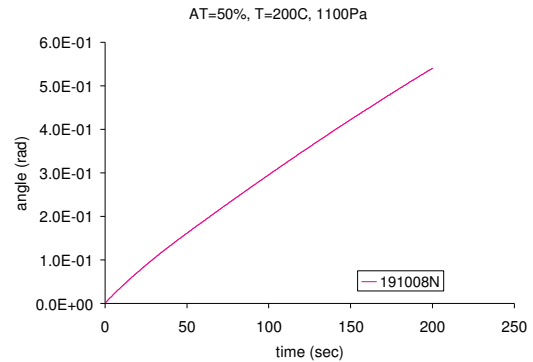
Fig 8. Output data from an individual rheometer test.

Clearly the data from the rheometer have to be adjusted for comparison with results from the pull through tests. The normal force, n, can be converted to normal pressure, P, by

$$P = n/A_o \qquad (1)$$

where A_o is the testing area (πR^2) and R is the radius of the truncated platen (see section 2.2). The angular velocity at any radius, r, can be converted to linear velocity (mm/s) using $v = \omega r$ where ω is the angular velocity (calculated from the gradient of the line shown in Fig. 8) and r is the radius. The linear velocity varies from zero at $r = 0$ to a maximum at $r = R$. The weighted average linear velocity is used to process the rheometer data for comparison against pull-through tests, i.e.

$$v = \frac{2}{3}\omega R \qquad (2)$$

Typical data generated by the rheometer tests at a temperature of 180°C, showing normal mass (the applied load measured in grams), m, versus linear velocity, v, for different imposed constant shear stresses are plotted in Fig. 9. Similar graphs were also produced for temperatures of 160°C, 200°C and 220°C (not shown here). Trend lines were fitted through the data. Each trend line was of exponential

4

form as in Eq (3). The average exponent, C_2, of all trend lines at different temperatures and shear stresses was found to be -1.37 with a standard deviation of 0.4. C_1 changed according to the different experimental conditions.

$$P = C_1 \cdot v^{C_2} \qquad (3)$$
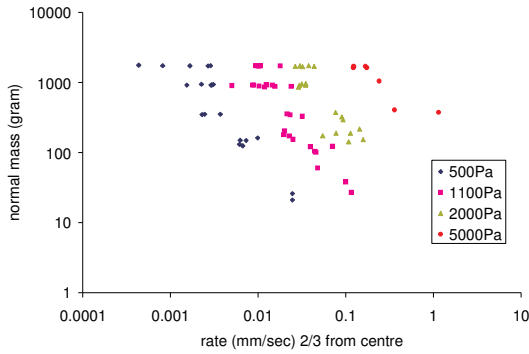
Fig. 9. Normal mass versus rate data generated for different shear stresses at 180°C.

Fig. 10 shows the data converted to normal pressure versus rate together with trend lines with C_2 = -1.37.
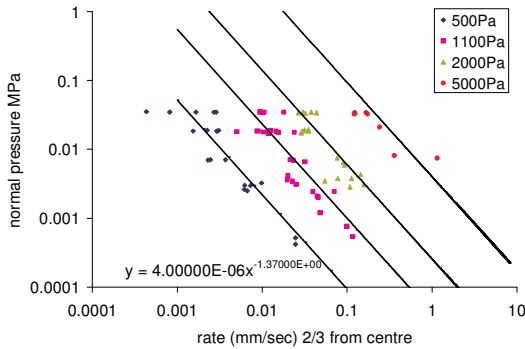
Fig. 10. Normal pressure versus rate data with trend lines of the form given in Eq (3) with C_2 = -1.37.

The general form of the final master curve is assumed to take the form

$$P = C_3 \cdot a_\tau \cdot a_T \cdot v^{-1.37} \qquad (4)$$

where a_τ is the shift factor for the shear stress and a_T is the shift factor for the temperature. It is possible to shift the data horizontally, vertically or by a combination of the two methods, the choice here is arbitrary. A vertical shifting was chosen. In order to determine the shift factors a reference temperature and reference shear stress had to be chosen (180°C and 500Pa). Eq (4) could then be written as

$$P = 4 \times 10^{-6} \cdot a_\tau \cdot a_T \cdot v^{-1.37} \qquad (5)$$

When a_τ and a_T both equal 1, Eq (5) gives the trend line of the reference data, the lowest trend line shown in Fig 9. Thus the factor $4 \times 10^{-6} = C_{3ref}$ and includes the conversion from normal mass to normal pressure. The constant C_3 of each trend line can be related to C_3 of the reference curve, i.e., C_{3ref}, simply by determining the ratio between the two, as shown in see Eq (6). Thus a_τ is the factor by which the reference curve must be multiplied in order to shift it to coincide with trend lines fitted to data produced at other shear stresses at the reference temperature. Evidently the size of a_τ is determined by the relative magnitudes of the shear stresses of the two curves. A relationship of the form shown in Eq (6) is postulated. The aim is to determine the value of the exponent b in Eq (6). Table 2 shows the information used to determine b.

$$a_\tau = \frac{C_3}{C_{3ref}} = \left(\frac{\tau}{\tau_{ref}}\right)^b \qquad (6)$$

Table 2. Information used to determine b in Eq (6)

Shear stress (Pa)	C_3	$\dfrac{\tau}{\tau_{ref}}$	$\dfrac{C_3}{C_{3ref}}$	b
500	$4.0 \cdot 10^{-6}$	1	1	-
1100	$4.25 \cdot 10^{-5}$	2.2	10.65	3
2000	$2.56 \cdot 10^{-4}$	4	64	3
5000	$4.0 \cdot 10^{-3}$	10	1000	3

Here $\tau_{ref} = 500 \times 10^{-6}$ MPa, a value of $b = 3$ was determined from the data, thus Eq (4) can be written as

$$P = 4 \times 10^{-6} \cdot \left(\frac{\tau}{500 \times 10^{-6}}\right) \cdot a_T \cdot v^{-1.37} \qquad (7)$$

When $a_T = 1$ Eq (7) can be used to determine P at 180°C for shear stresses between 500 and 5000 Pa. A similar equation was determined for the other temperatures though the factor C_3 in each case was different. In order to apply Eq (7) to other temperatures all that remains was to determine a_T where

$$a_T = \frac{P(T)}{P(T_{ref})} = \frac{C_3(T)}{C_3(T_{ref})} \qquad (8)$$

The relationship between a_T and temperature was assumed to follow an Arrhenius type behaviour, thus

$$\log(a_T) = A\left(\frac{1}{T} - \frac{1}{T_{ref}}\right) \qquad (9)$$

The aim here is to determine A. This can be determined by plotting $\log(a_T)$ versus ($1/T$-$1/T_{ref}$). Arrhenius type behaviour is indicated if the data follow a straight line. The data are plotted in Fig. 11.
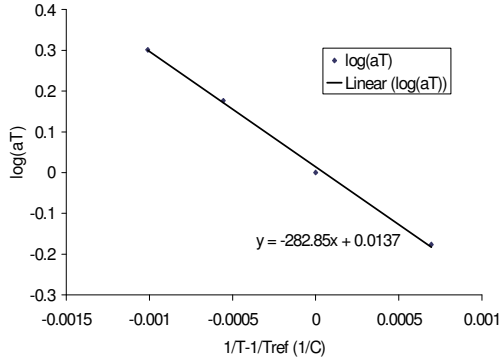
Fig 11. Determination of the gradient of the plotted data gives A in Eq (9)

A trend line fitted to the data gives A = -282.85. Thus, Eq (9) can be written

$$a_T = 10^{-282.85\left(\frac{1}{T} - \frac{1}{180}\right)} \qquad (10)$$

and substituted in Eq (7) to produce a general equation including rate, normal pressure and temperature. However, the equation requires further modification. This is because a Newtonian assumption is made when the rheometer converts the intended input shear stress to torque for the parallel plate geometry [12]. This problem has been addressed for non-Newtonian fluids [13] resulting in Eq (11), this can be used to correct the friction data

$$\tau = \frac{M}{2\pi R^3}\left[3 + \frac{d\ln M}{d\ln v}\right] \qquad (11)$$

where M is the applied torque. For a Newtonian fluid $d\ln M / d\ln v = 1$. For non-Newtonian fluid the term is less than 1. Using the rheometer data a value of approximately 0.39 was found. This results in a small modification to the Newtonian master curve, Eq (7) which can be rearranged as

$$\tau = 565 \times 10^{-6} \sqrt[3]{\frac{P \cdot v^{-1.37}}{4 \times 10^{-6} \cdot a_T}} \qquad (12)$$

where a_T is given by Eq (10) and τ is the shear stress in MPa, v is the velocity in mm/s, P is the normal pressure in MPa and T is the temperature in

°C. The shear stress can be converted to the friction force simply by multiplying by the area of the platen.

5 Analysis of results

Previous investigations [6,7,9,10] have attempted to analyse friction data in terms of a Stribeck curve, a plot of the coefficient of friction μ as a function of the Hersey number $H = \eta v/N$, where η is the viscosity of the lubricating fluid layer, v is the velocity in ms^{-1} and N is the normal force in N. The difficulty here is in determining the viscosity of the fluid layer. This is a non-Newtonian fluid (polypropylene) the viscosity of which depends on the shear rate, which in turn depends on the thickness of the fluid layer. Determining the thickness of this layer during shear is not easy. One option has been to make an estimate of this thickness using optical measurements taken from preconsolidated Twintex sheet. Values of 0.11 mm [9] and 0.07 mm [6,7] have been used. A comparison is made here between the pull-though rig data and the rheometer data using a Stribeck curve approach. To do this a film thickness of 0.11mm is assumed in order to find the shear rate. The PP matrix has been characterised previously and fitted with a Carreau-Yasuda model [15].
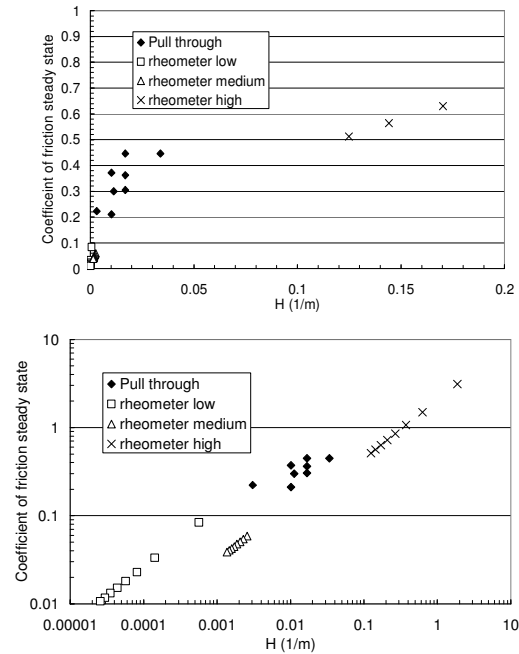
Fig 12. Top: data plotted on a linear scale, bottom: data plotted on a log-log scale.

Using this information the viscosity of the fluid layer can be estimated, although it should be noted that the rheological data are reliable only for relatively low shear rates ($<10s^{-1}$). In Fig. 12 the pull-through data shown in Table 1 are compared with data generated using Eq (12). The rheometer data were determined for low, medium and high Hersey numbers using the data sets shown in Table 3. Care was taken to generate rheometer data only within the working range of the rheometer. The velocity and temperature values were set and data generated by varying the normal force around the values shown in Table 3. The ability to measure at very low normal forces means that very high Hersey numbers can be reached.

Table 3. Parameter sets used to generate low, medium and high rheometer data.

	v (mm/s)	T (deg C)	N (N)
low	0.001	220	220
medium	0.05	190	50
high	1	160	0.5

Fig. 12 shows that the pull through test data lie within the envelope of the rheometer data. Also, the fact that the rheometer data can be generated away from a single curve may suggest that the rheometer data does not strictly follow the theoretical Stribeck behaviour. However, errors introduced by the fitting procedure and the assumption of a constant film thickness make it difficult to be certain.

6 Modelling

A meso-scale model has been developed at the University of Twente [9,10] based on a geometrical description of the tows within the fabric. One of the advantages of the model is that the film thickness can be predicted from the normal pressure and velocity. This avoids the use of the approximation of the film thickness required in the analysis of section 5. Fig. 13 presents a schematic cross section of the composite material in the warp direction. Hydrodyamic lubrication is assumed between the bundles and the tool surface. The total friction force per unit width follows by integrating the surface shear stresses over the length of the cross section, disregarding the bundle curvatures out of the plane for the time being. The contributions of the longitudinal warp and transverse weft yarns can be analysed separately and added up to the total friction force.
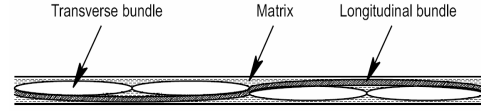
Fig. 13. Schematic cross section of a Twintex ply.

The Reynolds' equation describes the relation between the pressure and thickness distributions in thin film lubrication. The simple one dimensional steady state situation is given by

$$\frac{\partial}{\partial x}\left(\frac{h^3}{\eta}\frac{\partial p}{\partial x}\right) = 6U\frac{\partial h}{\partial x}. \tag{13}$$

A Cross-WLF viscosity model was used to characterise the steady shear viscosity [10]. The parameters of the model were taken from the literature [16] and the model predictions were found to give very good correspondence (slightly lower) with the Carreau-Yasuda model fitted to the actual PP viscosity data reported in [15]. The advantages of using the Cross-WLF model are the pressure dependence incorporated in the model and the reliability of the data at shear rates greater than $10\,s^{-1}$.

The pressure distribution can be solved for a given film thickness distribution using the following boundary conditions (see Fig. 14).

$$p(-L) = 0; \qquad p(x_0) = 0; \qquad \frac{\partial p}{\partial x}(x_0) = 0; \tag{14}$$

where the pressures are assumed to be non-negative due to cavitation in the fluid.
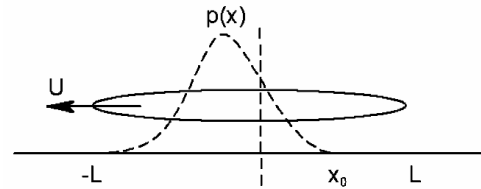
Fig. 14. Schematic pressure distribution underneath a bundle.

The bearing force per unit width is given by

$$F_B = \int_{-L}^{x_0} p(x)\,dx; \tag{15}$$

whereas the friction force per unit width follows as

$$F_f = \int_{-L}^{x_0} \tau(x)\,dx = \int_{-L}^{x_0} \frac{h}{2}\frac{\partial p}{\partial x} + \eta\frac{U}{h}\,dx. \tag{16}$$

The one dimensional mesoscopic model predicts the bearing and friction forces F_B and F_f with the

temperature T, velocity U and minimum film thickness h_0 as input parameters. The model was used inversely, iteratively adapting h_0 such that the integrated bearing force over all fibres was equal to the prescribed normal load N. This procedure also leads to the integral pull-out force, which can be compared to the experimental results.

In order to compare the meso-scale model with the master curve given by Eq (12) the tow geometry within the fabric described in section 2 must be modelled. The tows are characterised by an ellipse which is in turn approximated using polynomial functions. The width of the bundles or contact lengths have to be determined to calculate the bearing and friction forces. Table 4 shows the parameters used to characterise the tow geometries.

Table 4. Input values for the meso-scale model required to predict the empirical results characterised by Eq (12)

Parameter	Value	
Transverse bundle length	5.0	mm
Transverse bundle approximation	$y = 8 \cdot x^2$	
Longitudinal bundle length	10	mm
Longitudinal bundle approximation	$y = 16 \cdot x^2$	
Contact area	490	mm^2
Total number of contact areas	10	

Eq (12) is compared for three different normal forces, temperatures and pull out velocities. The values for the different parameters are displayed in Table 5. The meso-scale model predicts a different minimum film thickness for each experimental condition (noted in Table 5). This film thickness and the friction force predicted by the meso-scale model are presented in Table 5 along with the friction force predicted by the master curve, Eq (12). The comparison reveals a close correspondence between the model and master curve.

Table 5. Minimal film thicknesses ('h_m' in this table) and friction forces determined by the meso-scale model ('F_f model' in this table) together with predictions of Eq(12) ('F_f Nottingham' in this table)

T (°C)	U (mm/min)	N (N)	h_m (mm)	F_f model (N)	F_f Nottingham (N)
200	0.1	10	0.00124	0.219	0.228
200	1	10	0.01030	0.585	0.651
200	10	10	0.05150	1.550	1.860
180	1	20	0.00800	1.038	0.926
200	1	20	0.00505	0.835	0.821
220	1	20	0.00335	0.689	0.743
180	10	5	0.10400	1.484	1.669
180	10	10	0.06850	1.973	2.103
180	10	20	0.04200	2.666	2.649

The most interesting results of the comparison are presented in Fig. 15.
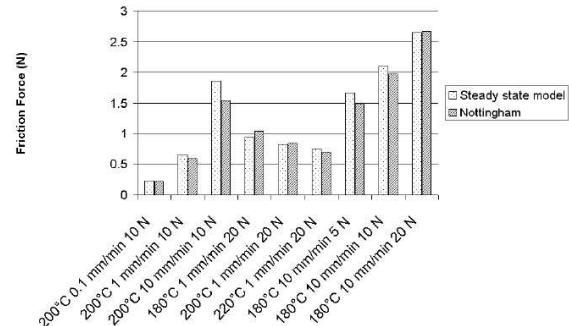
Fig 15. Comparison of Eq (12), indicated as 'Nottingham' in the legend, with the meso-scale model from [9]

The comparison shown in Fig. 15 is surprisingly close, showing excellent agreement over a range of temperatures and normal forces. Finally, master curves for different velocities and temperatures are plotted against the meso-scale model for different normal forces, see Fig. 16. Only at higher temperatures do the meso-scale predictions deflect away from the master curve, Eq (12).
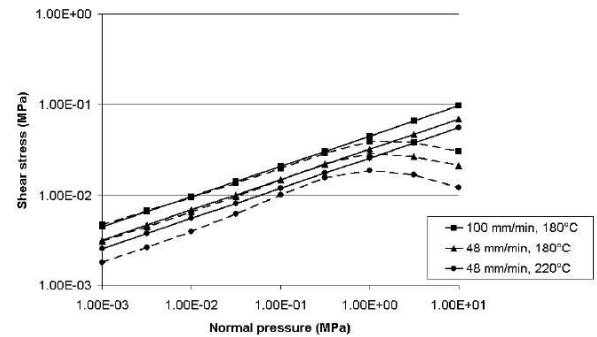
Fig. 16. Plots of Eq (12) together with predictions of the meso-scale model from Twente for different normal forces at different velocities and temperatures. The solid line represents Eq (12) and the dotted line the meso-scale model predictions.

6 Conclusions

A novel method of characterising the friction behaviour of viscous textile composites has been developed using a commercial rheometer and a custom designed set of platens. The rapid testing rate possible using the rheometer together with the more controllable experimental conditions make the test a useful addition to the current methods of

characterising the friction behaviour of viscous textile composites.

Pull through test data and rheometer data compare well when plotted as the coefficient of steady state friction versus Hersey number as is usual when plotting a Stribeck curve. The high sensitivity of the rheometer means that a wide range of Hersey numbers can be explored. Finally, a comparison between the recently developed meso-scale friction model from the University of Twente [9,10] and the master curve generated from the rheometer data show excellent agreement. This is very promising since the meso-scale model is based on the fabric geometry and matrix viscosity. This approach may considerably reduce the number of characterisation tests required for viscous textile composites in the future.

References

[1] Lin, H., Long, A.C., Clifford, M.J., Wang, J. and Harrison, P. *"Predictive Modelling of FE Forming to Determine Optimum Processing Conditions"*, *10th International ESAFORM Conference on Materials Forming*, 18th-20th April, Zaragosa, Spain, 1092-1097, 2007.

[2] Lin, H, Wang, J., Long, A.C., Clifford, M.J. and Harrison, P. "Predictive Modelling for Optimisation of Textile Composite Forming", *Composites Science and Technology* (in press), 2007.

[3] http://www.twintex.com Material data sheet Twintex®, 2004.

[4] Murtagh, A.M. "Surface friction effects related to pressforming of continuous fibre thermoplastic composites*". Composites Manufacturing*, 6, 169-175, 1995.

[5] Wilks, C.E. "*Processing technologies for woven glass polypropylene composites*". PhD thesis, University of Nottingham, 1999.

[6] Gorczyca-Cole, J.L., Sherwood, J.A. and Chen, J. "A friction model for use with a commingled glass-polypropylene plane weave fabric and the metal tool during thermostamping" *Revue Europeeanne des Elements Finis*. 729-751, 2005.

[7] Gorczyca-Cole, J.L., Sherwood, J.A. and Chen, J. "A friction model for thermostamping commingled glass-polypropylene woven fabrics" *Composites Part A*, 38, 393-406, 2007.

[8] Van de Haar K., "*Modelling resistance at the ply/tool contact interface for Twintex*®", MPhil thesis, Nottingham university, 2005.

[9] Ubbink, M., *"Tool ply friction of woven fabric composites*", Masters thesis, University of Twente, 2006.

[10] Akkerman, R., Ubbink, M.P., de Rooij, M.B. and ten Thije, R.H.W. "Tool-ply friction in composite forming", *10th International ESAFORM Conference on Materials Forming*, 18th-20th April, Zaragosa, Spain, 2007.

[11] Lin, H., Harrison, P., Van de Haar, K., Wang, J., Long, A.C., Akkerman, R., and Clifford, M.J. *"Investigation of Tool-Ply Friction of Textile Composites", 8th International Conference on Textile Composites (TEXCOMP)*, 16th-18th October, Nottingham, UK, 2006.

[12] *User Manual for Bohlin Rheometers*, Bohlin Instruments Ltd., page 183, 2001.

[13] Darby, R. "*Viscoelastic Fluids; An Introduction to Their Properties and Behaviour"*, in *Chemical Processing and Engineering* Marcel Dekker, Inc: New York and Basel, 638, 1976.

[14] Liu, L., Chen, J., Gorczyca, J. and Sherwood, J., "Modelling of friction and shear in thermoplastic composites"- Part I. *Journal of Composite Materials*, 38, 2004.

[15] Harrison, P., Clifford, M.J., Long, A.C. and Rudd, C.D. "A constituent-based predictive approach to modelling the rheology of viscous textile composites", *Composites: Part A*, 38, 7-8, 2004.

[16] *Moldflow Plastics Insight 5.0.* accessed on 30th August 2005.